Journal of Ceramic Processing Research. Vol. 24, No. 1, pp. 98~102 (2023)
(Received 29 June 2022, Received in revised form 13 August 2022, Accepted 3 September 2022)
https://doi.org/10.36410/jcpr.2023.24.1.98

J O U R N A L O F
Ceramic Processing Research

Structural and magnetic properties of M-type $Sr_{0.1}Ca_{0.4}La_{0.5}Fe_{12}O_{19}$ ferrites: The effects of $Co_xFe_{3-x}O_4$ in precursor

Xiubin Zhao[a], Shuang Zhang[a], Jinsong Li[a], Ailin Xia[a,*] and Yujie Yang[b]
[a]*School of Materials Science and Engineering, Anhui University of Technology, Maanshan 243002, China*
[b]*School of Materials Science and Engineering, Anhui University, Hefei 230601, China*

M-type ferrite $Sr_{0.1}Ca_{0.4}La_{0.5}Fe_{12}O_{19}$ magnetic powders doped with $Co_xFe_{3-x}O_4$ ($0 \le x \le 1.25$) in precursors were prepared by a ceramics process. The structure of specimens were examined by using an X-ray diffractometer. Only the magnetoplumbite phase was found in the specimens with the cobalt content (x) from 0.25 to 1.25 in precursor. The specimens exhibited a typical hexagonal M-type structure and the particles in specimens were uniformly distributed in size. The specimen with x=1.25 had the maximum saturation magnetization of 67.48 emu/g, while the residual magnetization and the coercivity of the specimen with x=1.00 reached the maximum value of 31.83 emu/g and 1270 Oe, respectively.

Keywords: M-type ferrite, Cobalt content, Ceramic method, Magnetic properties.

Introduction

M-type permanent magnetic ferrite ($SrFe_{12}O_{19}$, SrM) is widely used due to its relatively high saturation magnetization (M_s) and coercivity (H_c). Besides, it has fine magnetocrystal anisotropy constant, excellent corrosion resistance and chemical stability [1-4]. Currently, some metal ions, such as Co^{2+}, La^{3+}, Ca^{2+}, Cu^{2+}, La^{3+}-Co^{2+}, La^{3+}-Zn^{2+} and so on, are substituted or doped into the SrM ferrites attempting to improve the magnetic properties for the sake of special application [5-20]. Kools et al. [16] studied the structural and magnetic properties of M-type ferrite doped by La-Co ions. It was found that Co^{2+} ions replaced Fe^{3+} ions on octahedral lattice points $4f_2$ and 2a, and the magnetic properties were improved through the $4f_2$ substitution. A.L. Xia et al. [17] prepared the $SrFe_{12}O_{19}$-$CoFe_2O_4$ nanocomposites by using a hydrothermal method. The study found that compared with single-phase $SrFe_{12}O_{19}$, when the exchange coupling appeared, with the increasing content of $CoFe_2O_4$, the M_s of composites increased significantly from 59.2 emu/g to 72.4 emu/g. W.C. Li et al. [18] prepared La-Co substituted $Sr_{1-x}La_xFe_{12-x}Co_xO_{19}$ ferrite via a sol-gel combustion method. It was found that the M_s reached the maximum value when the La-Co substitution was x=0.3. S.M. Masoudpanah et al. [19] prepared the La-Co substituted M-type ferrite thin films by using laser deposition. The results showed that the M_s increased first and then decreased with the increasing La-Co amount. Y. Liu et al. [20] prepared the La-Co substituted M-ferrite by co-improved precipitation and molten salt method, and the results showed that the M_s and H_c were comparable to those synthesized via a high-temperature method. However, the influence of different cobalt content in precursor on the magnetic properties of SrM ferrites is still not reported. Through this study, it may help enterprises reduce the use of rare earth elements in production

In this study, the SrM magnetic powders were obtained via a ceramic process with different $Co_xFe_{3-x}O_4$ ($0 \le x \le 1.25$) precursors. The effects of the cobalt content (x) in precursor on the structural and magnetic properties of specimens were studied.

Experimental Procedures

Preparation of $Co_xFe_{3-x}O_4$ ($0 \le x \le 1.25$) precursors

All specimens with a nominal composition of $Co_xFe_{3-x}O_4$ ($0 \le x \le 1.25$ with steps of 0.25) were obtained via a traditional ceramic process. All the chemical reagents used were analytically pure (Fe_2O_3 and Co_2O_3). The mixed powders (Fe_2O_3 and Co_2O_3) were ball-milled in water for 2 h, and then the powders obtained were dried, sifted and sintered at 850 °C for 3 h in air. Finally, the sintered samples were pulverized to powders with a size of smaller than 100 μm.

Preparation of M-type ferrite $Sr_{0.1}Ca_{0.4}La_{0.5}Fe_{12}O_{19}$ powders with different cobalt content in precursor

All the $Sr_{0.1}Ca_{0.4}La_{0.5}Fe_{12}O_{19}$ powder specimens with different $Co_xFe_{3-x}O_4$ ($0 \le x \le 1.25$) precursors were obtained by using a ceramic process. The analytically

*Corresponding author:
Tel : +86 13665557919
Fax: +86 05552311570
E-mail: alxia@126.com

pure Fe_2O_3 (98% purity), $SrCO_3$ (98% purity), $CaCO_3$ (99% purity) and La_2O_3 (99% purity) were used as raw materials to prepare SrM ferrites. The mixed powders were milled for 2 h, together with $Co_xFe_{3-x}O_4$ of 3 wt%. The obtained powders were dried, sifted, and then sintered at 1300 °C for 2 h in the air atmosphere in a muffle furnace. Finally, the sintered specimens were pulverized to powders with a size of smaller than 100 μm.

Characterization

The phase identification of specimens was obtained on a PANalytical X'Pert Pro diffractometer (Almelo, Netherlands) using Cu K_α (λ = 1.5406 Å) radiation. The morphologies were examined by a HITACHI S-4800 field emission scanning electron microscopy (FESEM, Tokyo, Japan). The room temperature (RT) magnetic hysteresis loops of specimens were measured on a MicroSense EZ7 vibrating sample magnetometer (VSM) with a maximum external field of 20,000 Oe.

Results and Discussion

Structural and morphological properties

Fig. 1 shows the XRD patterns of SrM specimens obtained with different cobalt content (x) from 0 to 1.25 in precursors. As shown, in the specimens with x from 0.25 to 1.25, only typical peaks from single-phase magnetoplumbite SrM was found, which implies that the Co^{2+} ions entered into the magnetoplumbite lattice without producing any second phase.

The lattice constants a and c can be calculated using the values of Miller indices (h, k, l) and the inter-planer spacing d_{hkl} corresponding to (107) and (114) peaks according to the following formula (1):

$$d_{hkl} = \left(\frac{4}{3} \cdot \frac{h^2 + hk + k^2}{a^2} + \frac{l^2}{c^2} \right)^{-1/2} \quad (1)$$

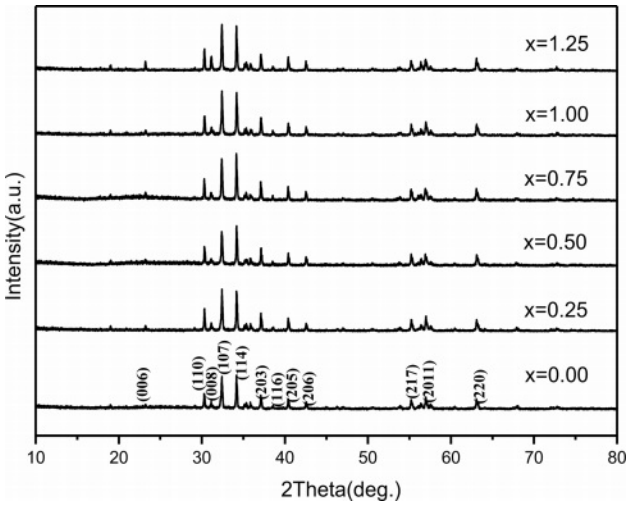

Fig. 1. XRD patterns of specimens obtained with different x.

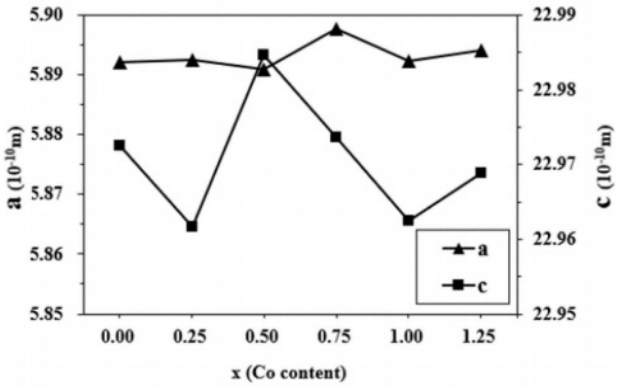

Fig. 2. The lattice constants a and c of specimens with different cobalt content (x).

The variations of lattice constants a and c of the specimens with different cobalt content (x) are shown in Fig. 2. It can be found that the c decreases slightly from 22.9725 Å (x=0.00) to 22.9616 Å (x=0.25). When the x ranges from 0.25 to 0.50, the c increases to 22.9847 Å. With a further increase of x from 0.50 to 1.00, the c decreases to 22.9624 Å. From 1.00 to 1.25, the c increases to 22.9689 Å. However, compared with c, the variation of a is not obvious, suggesting that the x affected c more greatly. This may result from the different distribution of Co ions.

Fig. 3 indicates the change of crystal axis ratio of c/a in different specimens. The c/a is approximately the same in Fig. 3. On the basis of Verstegen and Stevels [26], the value of c/a ratio may present the structure type. For the M-type structure, the ratio was assumed to be smaller than 3.98. Herein, the values of c/a ratio for the specimens range from 3.8954 to 3.9018, which seems to be in well accord with the reported range of M-type structure.

Figure 4 shows the typical FESEM images of specimens. As shown in Fig. 4, all the specimens

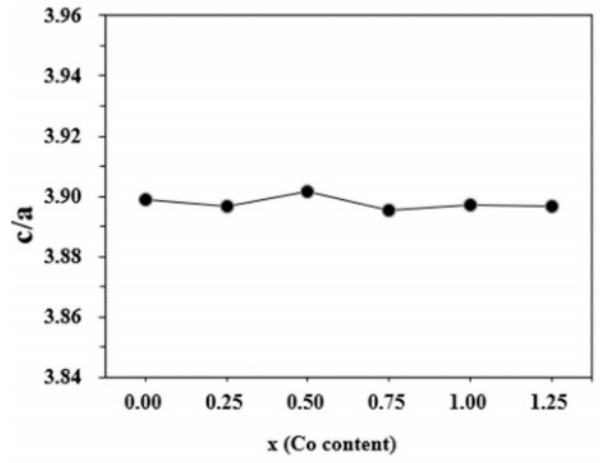

Fig. 3. The crystal axis ratio of c/a in the specimens with different x.

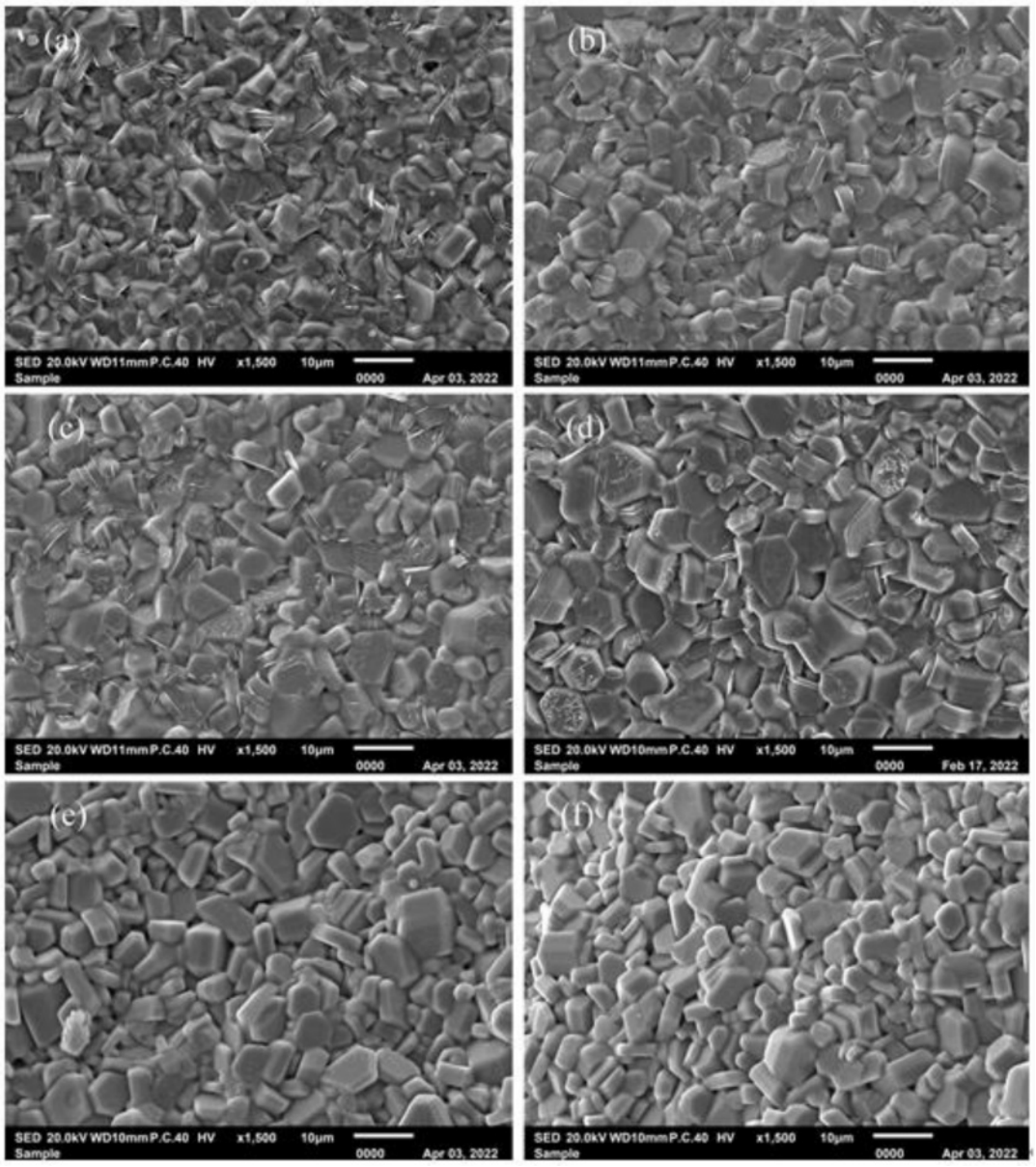

Fig. 4. Typical SEM images of specimens with different *x*. *x*: (a) 0, (b) 0.25, (c) 0.50, (d) 0.75, (e) 1.00 and (f) 1.25.

consist of the relatively uniform particles with typical hexagonal structure. It can be found that the average particle size of specimen with $x = 0$ is obviously smaller than those of specimens with $x > 0$. However, with the increasing x, the typical morphology and the average particle size of specimens did not change obviously.

Magnetic properties

Fig. 5 shows the RT magnetic hysteresis loops of specimens with different x. The M_s, H_c and residual magnetization (M_r) of specimens with different x were determined from Fig. 5 and are listed in Table 1. What should be pointed out is that since the magnetic hysteresis loops were roughly saturated at a field of 20 kOe, the value of magnetization obtained at 20 kOe can

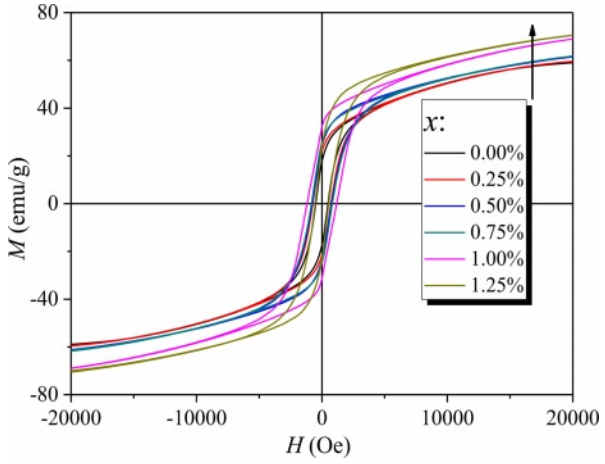

Fig. 5. RT magnetic hysteresis loops of specimens with different cobalt content (*x*).

Table 1. Magnetic properties of specimens with different cobalt content (x).

Cobalt content (x)	M_s (emu/g)	M_r (emu/g)	H_c (Oe)
0.00	56.88	17.54	518
0.25	57.45	21.91	775
0.50	59.06	23.88	830
0.75	59.25	25.24	902
1.00	66.20	31.83	1270
1.25	67.48	23.61	582

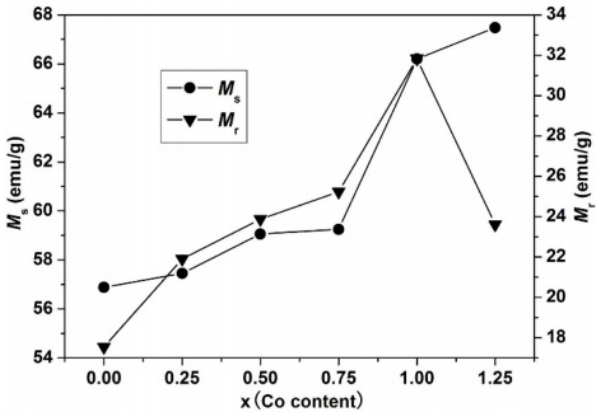

Fig. 6. The M_s and M_r of specimens with different cobalt content (x).

approximately be used as M_s.

As can be seen from Table 1 and Fig. 6, the M_s of specimens increases with the increase of x from 0 to 1.25, and it reaches 67.48 emu/g when x=1.25. The M_r of specimens increases with the increase of x from 0 to 1.00. When x increased from 1.00 to 1.25, the M_r decreases, and the maximum value is 31.83 emu/g (x=1.00). It is evident that the H_c has the same feature as M_s as shown in Table 1 and Fig. 7. The specimen with x=1.00 exhibits the best magnetic properties,

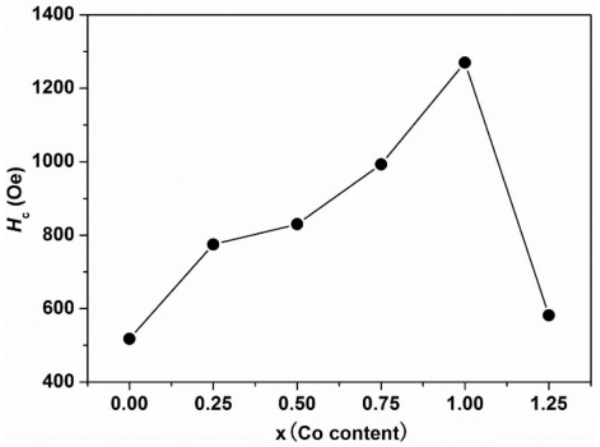

Fig. 7. The H_c of specimens with different x.

including the M_s (66.2 emu/g), the M_r (31.83 emu/g) and the H_c (1270 Oe). The variation of M_s and H_c with different x is in agreement with those reported in Ref. [17] and Refs. [20-21], respectively. However, the M_s, the M_r and the H_c of specimens are lower than those reported by Rashad et al. [27]. The Mössbauer investigations of La–Co-substituted M-type ferrites revealed that La^{3+} ions can replace the most Sr^{2+} ions, and a valence change of some Fe^{3+} to Fe^{2+} ions occurred in the 2a and $4f_2$ sites, while Co^{2+} ions mainly replaced Fe^{3+} at $4f_2$ octahedral sites [22-24]. When x is smaller (larger) than 1.0, the magnetic moment difference caused by Co substitution is positive (negative), respectively, resulting in the M_r of specimen increases first and then decreases with the increase of x.

G. Asti et al. [25] found that the magnetocrystal anisotropy field of ferrite increased with the increase of cobalt content, and the Mössbauer spectrum analysis of ferrite revealed that when the content of cobalt substitution is within a certain range, most of the Co^{2+} ions will substitute Fe^{3+} ions in $4f_2$ and $2a$ octahedral sites. The magnetocrystal anisotropy constant K_1 increases with the increase of cobalt content (x), and consequently the H_c was enhanced. With the increasing ratio of x, Co^{2+} replaces Fe^{3+} ions at 2b octahedral sites, thus reducing K_1 and H_c.

Conclusions

The M-type $Sr_{0.1}Ca_{0.4}La_{0.5}Fe_{12}O_{19}$ ferrite powders were obtained via a ceramic process with different $Co_xFe_{3-x}O_4$ ($0 \le x \le 1.25$) precursors. The XRD patterns showed that the single magnetoplumbite phase was obtained in all the specimens. The SEM study manifested that the particles were distributed uniformly in the specimens. The VSM study indicated the M_s of specimens increased with the increasing x from 0 to 1.25, and reached the maximum value at x=1.25, while the M_r of specimens increased with the increasing x from 0 to 1.25. The specimen with x=1.00 exhibited the best magnetic properties of M_s=66.2 emu/g, M_r =31.83 emu/g and H_c=1270 Oe. The cost of SrM may be reduced through tailoring the content of Co to reduce the usage of rare earth elements.

References

1. Y.J. Yang, F.H. Wang, and D.H. Huang, J. Magn. Magn. Mater. 452 (2018) 100-107.
2. A.L. Xia, T. Zhan, and R. Sun, J. Alloy. Compd. 784 (2019) 276-281.
3. M. Manikandan and C. Venkateswaran, J. Magn. Magn. Mater. 358-359 (2014) 82-86.
4. R.C. Pullar, Prog. Mater. Sci. 57 (2012) 1191-1334.
5. Y.J. Yang, X.S. Liu, and S.J. Feng, Chinese. J. Phys. 63 (2020) 337-347.
6. W.C. Li, X.J. Qiao, and M.Y. Li, Mater. Res. Bull. 48

(2013) 4449-4453.
7. T.P. Xie, L.J. Xu, and C.L. Liu, Powder. Technol. 232 (2012) 87-92.
8. C.A. Herme, P.G. Bercoff, and S.E. Jacobo, Mater. Res. Bull. 47 (2012) 3881-3887.
9. Y.Q. Li, Y. Huang, S.H. Qi, F.F. Niu, and L. Niu, J. Magn. Magn. Mater. 323 (2011) 2224-2232.
10. A. Thakur, R.R. Singh, and P.B. Barman, J. Magn. Magn. Mater. 326 (2013) 35-40.
11. Y.J. Yang, J.X. Shao, and F.H. Wang, J. Ceram. Process. Res. 18 (2017) 242-246.
12. Y.J. Yang and J.X. Shao, J. Ceram. Process. Res. 18 (2017) 394-398.
13. M.J. Iqbal, M.N. Ashiq, and I.H. Gul, J. Magn. Magn. Mater. 322 (2010) 1720-1726.
14. A. Cavalieri, T. Caronna, and I. Natali Sora, Ceram. Int. 38 (2012) 2865-2872.
15. M.J. Iqbal and M.N. Ashiq, Chem. Eng. J. 136 (2008) 383-389.
16. F. Kools, A. Morel, and R. Grössinger, J. Magn. Magn. Mater. 242-245 (2002) 1270-1276.
17. A.L. Xia, S.Z. Ren, and J.S. Lin, J. Alloy. Compd. 653 (2015) 108-116.
18. W.C. Li, X.J. Qiao, and M.Y. Li, Mater. Res. Bull. 48 (2013) 4449-4453.
19. S.M. Masoudpanah, S.A.S. Ebrahimi, and C.K. Ong, J. Magn. Magn. Mater. 342 (2013) 134-138.
20. Y. Liu. M.G.B. Drew, and Y. Liu, J. Magn. Magn. Mater. 322 (2010) 3342-3345.
21. T. Kikuchi and T. Nakamura, J. Magn. Magn. Mater. 322 (2010) 2381-2385.
22. P. Tenaud, A. Morel, and F. Kools, J. Alloy. Compd. 370 (2004) 331-334.
23. L. Lechevallier, J.M. Le Breton, and J.F. Wang, J. Phys-Condens Mat. 16 (2004) 5359-5376.
24. L. Lechevallier and J.M. Le Breton, Physica B. 327 (2003) 135-139.
25. G. Asti, F. Bolzoni, and J.M. Le Breton, J. Magn. Magn. Mater. 272-276 (2004) e1845-e1846.
26. G.B. Teh, Y.C. Wong, and R.D. Tilley, J. Magn. Magn. Mater. 323 (2011) 2318-2322.
27. M.M. Rashad and I.A. Ibrahim, J. Mater. Sci-Mater. El. 22 (2011) 1796-1803.